Available online at www.sciencedirect.com

ScienceDirect

Procedia Structural Integrity 25 (2020) 400–412

Structural Integrity Procedia

www.elsevier.com/locate/procedia

1st Virtual Conference on Structural Integrity - VCSI1

Nonlinear analysis of microscopic instabilities in fiber-reinforced composite materials

Umberto De Maio, Fabrizio Greco*, Lorenzo Leonetti, Andrea Pranno, Girolamo Sgambitterra

Department of Civil Engineering, University of Calabria, Via P. Bucci Cubo39B, Rende 87036, Italy

Abstract

Failure induced by fiber microbuckling is a frequent failure mode in continuous fiber-reinforced composite materials subjected to compression along the fibers direction. This failure mechanism may lead to a notable decrease of the compressive strength of composite materials since may also induce the initiation and propagation of cracks at the micro-structural level. A detailed microscopic continuum analysis with an appropriate representation of different sources of nonlinearities is usually required to capture the effects of different microscopic failure modes (instability, fracture damage, for instance), at the expense of a very large computational effort. In order to avoid a direct modeling of all microstructural details of the composite solid, micromechanically based multiscale techniques can be adopted in coupling with first order homogenization schemes. To this end a semiconcurrent two-scale approach is proposed in which the macroscopic constitutive law is evaluated resolving a micromechanical BVP in each macroelement of the homogenized domain; the microscopic model adopts a full finite deformation continuum formulation to study the interaction between local fiber buckling and matrix or fiber/matrix interface microcracks in presence of unilateral self-contact between crack surfaces. Numerical results are obtained to provide accurate predictions of the critical load level associated to microscopic instabilities in 2D fiber-reinforced composite solids.

Keywords: Fiber-reinforced composite; Finite strain homogenization; Self-contact mechanics; Buckling instability; Multiscale analysis.

* Corresponding author. Tel.: +390984496916.
E-mail address: fabrizio.greco@unical.it

10.1016/j.prostr.2020.04.045

Nomenclature

$\boldsymbol{u}_{\Gamma_{c(i)}}$	Displacement jump at the deformed crack contact interface at a contact point pair $\left(\boldsymbol{X}^l, \boldsymbol{X}^u\right)_C$
∂V	External RVE boundary in the deformed configuration
$\partial V_{(i)}$	External RVE boundary in the undeformed configuration
$\boldsymbol{C}^R\left(\boldsymbol{X}, \boldsymbol{F}\right)$	Fourth-order tensor of nominal moduli
$R\left(\dot{\bar{\boldsymbol{F}}}, \dot{\boldsymbol{w}}_1, \dot{\boldsymbol{w}}_2\right)$	Functional associated to the non-bifurcation condition
$H^1\left(V_{\#}\right)$	Hilbert space of order one of vector valued functions periodic over V
H_f	Initial fiber thickness
$dS_{(i)}$	Surface elements in the undeformed configuration
$\boldsymbol{x}\left(\boldsymbol{X}, t\right)$	Microscopic deformation field
$S\left(\bar{\boldsymbol{F}}, \dot{\boldsymbol{w}}\right)$	Stability functional
$\boldsymbol{r}_R{}^u$ $\left(\boldsymbol{r}_R{}^l\right)$	Nominal contact reaction on the upper (lower) crack surface
$\boldsymbol{T}_R(\boldsymbol{X})_{\Gamma_c(i)}$	Nominal stress tensor jump at the undeformed crack contact interface
$\boldsymbol{t}_R$	Nominal traction vector
$\dot{u}_n(\boldsymbol{X})_{\Gamma_c}$	Normal displacement rate jump at the deformed crack contact interface at a contact point pair
$\dot{w}_n(\boldsymbol{X})_{\Gamma_c}$	Normal fluctuation rate jump at the deformed crack contact interface at a contact point pair
$\boldsymbol{n}_{(i)}$	Outward normal at $\boldsymbol{X} \in \partial V_{(i)}$
t_c^M	Primary instability load level in a multiscale model
t_c^D	Primary instability load level in a direct model

1. Introduction

Over the past decade, scientific and industrial communities have shared their expertise to improve mechanical and structural design favoring the exploration and development of new technologies, materials and advanced modeling methods with the aim to design structures with the highest structural performances. The most promising materials are fiber- or particle-reinforced composite materials. Specifically, materials with periodically or randomly distributed inclusions embedded in a soft matrix offer excellent mechanical properties with respect to traditional materials (for instance, the capability to undergo large deformations). Recent applications of these innovative materials are advanced reinforced materials in the tire industry, nanostructured materials, high-performance structural components, advanced additive manufactured materials in the form of bio-inspired, functional or metamaterials. Both industrial and scientific communities are conscious that designing new complex structures and systems that simultaneously need to meet restrictive security, mechanical and, in some instances, economical constraints can only be accomplished by numerical simulations. Even though significant progress has been made in simulating different phenomena, more developments are still needed. This is particularly true for the computational techniques and algorithms used to investigate the behavior of materials with a heterogeneous microstructure and subjected to complex loading conditions.

Ideally, models able to simulate the behavior of advanced composite materials should be accurate and simple at the same time, so that they can be implemented in standard finite element packages to solve interesting structural issues. The development of accurate modeling strategies represents a significant challenge for two main reasons: firstly, the common constitutive models adopted to model advanced composite materials are nonlinear; secondly, due to the finite geometry changes caused by loadings, there is an additional complication related to the microstructural evolution.

This context motivates the requirement to carry out theoretical studies focused on the finite strain behavior of such materials with special attention to the prediction of the onset of microscopic failure mechanisms by investigating their macroscopic (homogenized) behavior. As a matter of fact, the study of such failure mechanisms requires the use of sophisticated techniques because otherwise a direct modeling of all microstructural details is needed which, however, is unpractical due to the required large computational effort. Among the variegated failure mechanisms affecting composite materials subjected to large deformations, loss of composite integrity (fracture, delamination and damage) and local buckling or loss of microscopic stability are the most common ones.

As regards the loss of composite integrity, in order to take account for microstructural evolution (such as crack propagation), different approaches can be adopted. In the past literature such approaches have been proposed within the context of small deformations but they have been also generalized to large deformations. Frequently they are implemented in conjunction with first-order homogenization methods (see, for instance, (Bruno et al., 2008; Greco, 2009; Li et al., 2004)) and/or multi-scale schemes (e.g. (Feo et al., 2015; Feyel and Chaboche, 2000; Greco et al., 2015, 2014; Yu et al., 2013)). Generally speaking, the homogenization approaches can be adopted if the assumptions of periodicity and scale separation are satisfied, whereas multiscale schemes overcome these limitations (such as the semiconcurrent, concurrent, hierarchical or hybrid methods, see for instance (Greco et al., 2020)), and they are able to accurately take into account for microstructural evolution due to coalescence of micro-cracks and to material and/or geometrical nonlinearities. Failure of fiber-reinforced composite materials is usually promoted by the pre-existence of microstructural defects, especially in the form of fiber/matrix debonding, as a consequence of the well-known stress concentration arising in bimaterial systems with higher elastic mismatches (see, for instance, (Fantuzzi et al., 2018; Tuna et al., 2019)). Further numerical analysis, for both the nucleation and propagation of multiple cracking in reinforced quasi-brittle materials, based on inter-element cohesive approaches, are discussed in (De Maio et al., 2019a, 2019b, 2019c). Regards to the loss of microscopic stability, in the case of undefected composite materials several theoretical and numerical studies on the occurrence of instabilities at the scale of the microstructure have been performed in the literature, in order to determine the influence of these phenomena on the nonlinear macroscopic response of the composite solid, see for instance (Greco and Luciano, 2011; Michel et al., 2010; Miehe et al., 2002; Nestorović and Triantafyllidis, 2004; Nezamabadi et al., 2009). Generally speaking instability phenomena strongly reduce the structural integrity of structures , thus it must be investigated at different length scales (see, for instance, (Michel et al., 2010; Miehe et al., 2002)), and also, both geometrical and constitutive nonlinearities must be incorporated in the analysis (see, for instance, (Greco and Luciano, 2011)).

Subsequently the pioneering study of (Triantafyllidis and Maker, 1985) devoted to the connections between microscopic and macroscopic instabilities in hyperelastic layered composites materials with a periodic microstructure, such nonlinear aspects were rigorously investigated in (Geymonat et al., 1993), where it was shown that instabilities with long wavelength lead to the loss of strong ellipticity condition of the unit cell homogenized moduli tensor and, as consequence, to a macroscopic instability. Following the above-mentioned works, the interrelationships between microscopic and macroscopic instabilities under plane-strain condition in hyperelastic periodic composites (layered and particle-reinforced) have been widely investigated in (Li et al., 2019; Slesarenko and Rudykh, 2017), by using the Bloch-Floquet technique in a FEM framework. The above investigations showed that the onset of the macroscopic instabilities (characterized by wavelengths significantly larger than the microstructure characteristic size) can be predicted by the loss of ellipticity analysis, whereas the prediction of instabilities with a small wavelength (local instability modes) requires sophisticated techniques such as Bloch wave stability analysis or direct finite element discretization of the unit cell assembly leading to a impracticable computational efforts due to the theoretically infinite nature of the analysis domain. In addition, to obtain a conservative prediction of the microscopic stability region with a lower computational effort the macroscopic constitutive stability measures shown in (Greco and Luciano, 2011) can be adopted.

In composite materials subjected to large deformations, since the above studies were prevalently limited to the investigation of microscopic and macroscopic instabilities in undefected microstructures, the problem of interaction between different microscopic failure modes has been scarcely investigated, although it may have a detrimental effect on the overall failure response of composite materials. Furthermore, a detailed continuum analysis of composite solids taking into account the coupling effects between microfractures and microinstabilities requires a huge computational effort since a sophisticated numerical model must be adopted in order to accurately describe the different sources of nonlinearity (for instance those related to damage, constitutive and geometrical effects). The above considerations

motivate the requirement to conduct theoretical studies focused on the understanding of the finite strain behavior of such materials giving great attention to the prediction of the onset of microscopic failure mechanisms by investigating their nonlinear homogenized behavior in a multiscale framework.

2. Theoretical formulation of the microscopic stability analyses in damaged fiber-reinforced composite by using homogenization techniques

The considered microstructured solid consists of a periodic fiber reinforcement embedded in a microcracked matrix and the equilibrium problem is formulated with reference to the representative volume element (RVE) shown in Fig.1. The volume occupied by the homogenized composite in the initial configuration and the position vector of a generic macroscopic point are referred to as $\overline{V}_{(i)}$ and $\boldsymbol{X}$, respectively. The RVE is assumed to contain pre-existing cracks whose upper and lower surface are denoted as $\Gamma^{u}_{(i)}$ and $\Gamma^{l}_{(i)}$, in which the superscript u and l are respectively referred to upper and lower surface and the subscript (i) is referred to the initial configuration. With the aim to predict the stability phenomena the considered RVE may be composed by an assembly of periodic unit cells a-priori unknown or by a single unit cell (see, for instance, (Geymonat et al., 1993)). On the undeformed configuration, a generic point is identified with its position vector $\boldsymbol{X}$ and the nonlinear deformation of the microstructure is denoted by $\boldsymbol{x}(\boldsymbol{X})$ mapping points $\boldsymbol{X}$ of the initial configuration $V_{(i)}$ onto points $\boldsymbol{x}$ of the actual configuration V. The displacement field is defined as $\boldsymbol{u}(\boldsymbol{X})=\boldsymbol{x}(\boldsymbol{X})-\boldsymbol{X}$ and the deformation gradient is defined as $\boldsymbol{F}(\boldsymbol{X})=\partial\boldsymbol{x}(\boldsymbol{X})/\partial\boldsymbol{X}$ each microconstituents of the RVE follow a rate independent incrementally linear constitutive law that can be written in following form:

$$\dot{\boldsymbol{T}}_R=\boldsymbol{C}^R(\boldsymbol{X},\boldsymbol{F})\left[\dot{\boldsymbol{F}}\right] \tag{1}$$

where $\dot{\boldsymbol{T}}_R$ and $\dot{\boldsymbol{F}}$ represents the rate of the first Piola-Kirchhoff stress tensor and the rate of the deformation gradient, respectively, and $\boldsymbol{C}^R$ is the corresponding fourth-order tensor of nominal moduli satisfying the major symmetry condition : $C^R_{ijkl}=C^R_{klij}$. The loading process is parametrized in terms of the time-like parameter monotonically increasing $t\geq 0$ (t = 0 in the undeformed configuration). Such parameter produces a unique response defined as principal equilibrium path and, since it describes the quasi-static deformation path of the composite solid, the rates of field quantities are considered to be the derivative with respect it.

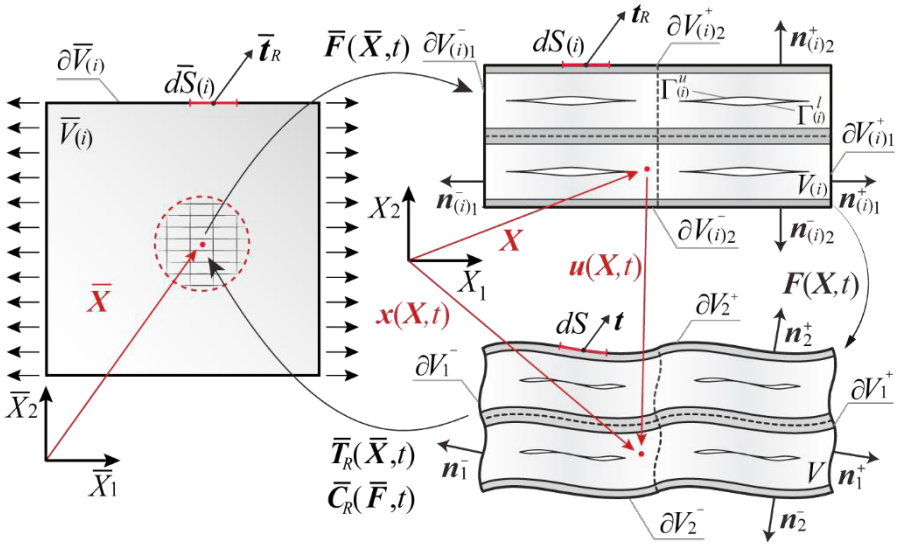

Fig. 1. Homogenized solid of a microcracked fiber-reinforced composite material (to the left) and corresponding undeformed and deformed RVE configurations (to the right) attached to a generic material point.

For hyperelastic materials the constitutive behavior is derived from a strain energy-density function $W(\boldsymbol{X},\boldsymbol{F})$, and thus the nominal stress tensor (second-order tensor) and the nominal moduli tensor (fourth-order tensor) can be defined as:

$$\boldsymbol{T}_R = \frac{\partial W(\boldsymbol{X},\boldsymbol{F})}{\partial \boldsymbol{F}},\ \boldsymbol{C}^R(\boldsymbol{X},\boldsymbol{F}) = \frac{\partial^2 W(\boldsymbol{X},\boldsymbol{F})}{\partial \boldsymbol{F}\partial \boldsymbol{F}} \tag{2}$$

whose components are respectively $T_{R\,ij} = \partial W(\boldsymbol{X},\boldsymbol{F})/\partial F_{ij}$ and $C^R_{ijkl} = \partial^2 W(\boldsymbol{X},\boldsymbol{F})/\partial F_{ij}\partial F_{kl}$. The coupling relationship characterizing the microscopic and the macroscopic scales can be expressed in terms of boundary displacement and traction vector defining, as follow, the macroscopic deformation gradient $\bar{\boldsymbol{F}}$ and the first Piola-Kirchhoff stress tensor $\bar{\boldsymbol{T}}_R$:

$$\begin{aligned} \bar{\boldsymbol{F}}(t) &= \frac{1}{|V_{(i)}|}\int_{\partial V_{(i)}} \boldsymbol{x}(\boldsymbol{X},t)\otimes \boldsymbol{n}_{(i)} dS_{(i)} \\ \bar{\boldsymbol{T}}_R(t) &= \frac{1}{|V_{(i)}|}\int_{\partial V_{(i)}} \boldsymbol{t}_R(\boldsymbol{X},t)\otimes \boldsymbol{X} dS_{(i)} \end{aligned} \tag{3}$$

where $\boldsymbol{n}_{(i)}$ denotes the outward normal at $\boldsymbol{X}\in\partial V_{(i)}$, $\otimes$ denotes the tensor product and $\boldsymbol{t}_R = \boldsymbol{T}_R\boldsymbol{n}_{(i)}$ represents the first Piola-Kirchhoff traction vector. In a macrostrain driven loading regime, the microscopic deformation field can be written as a function of the macro-deformation gradient $\bar{\boldsymbol{F}}(t)$ and of the fluctuation field $\boldsymbol{w}(\boldsymbol{X},t)$ as follow:

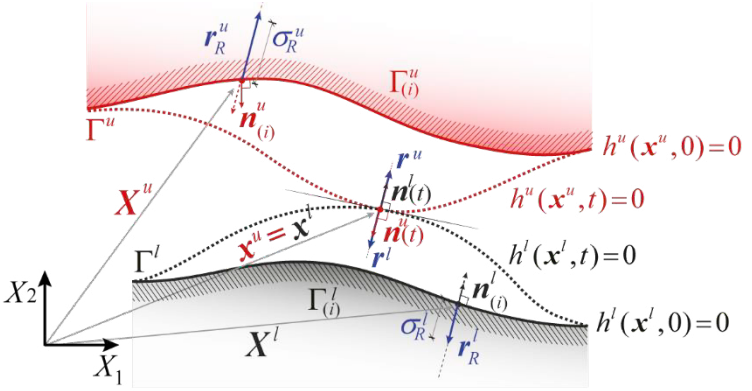

Fig. 2. Undeformed and deformed configurations of the crack surfaces, highlighting the pair of crack surface points $(\boldsymbol{X}^l,\boldsymbol{X}^u)_C$ and the main associated parameters.

$$\boldsymbol{x}(\boldsymbol{X},t) = \bar{\boldsymbol{F}}(t)\boldsymbol{X} + \boldsymbol{w}(\boldsymbol{X},t) \tag{4}$$

where $\bar{\boldsymbol{F}}(t)\boldsymbol{X}$ represents a linear displacement contribution. The application of (3) to the boundary of the RVE leads to the following integral constraint written in terms of RVE boundary displacements:

$$\int_{\partial V_{(i)}} \boldsymbol{w}\otimes \boldsymbol{n}_{(i)} dS_{(i)} = \boldsymbol{0}. \tag{5}$$

Such boundary constraint is automatically satisfied assuming that the microstructure is periodic, it leads to consistent displacements of opposing boundary; in particular, this condition establishes a split of the boundary limits in a positive part $\partial V_{(i)}^+$ and in a negative part $\partial V_{(i)}^-$:

$$\partial V_{(i)} = \partial V_{(i)1}^+ \cup \partial V_{(i)2}^+ \cup \partial V_{(i)1}^- \cup \partial V_{(i)2}^-; \tag{6}$$

The corresponding outward unit vectors $\boldsymbol{n}^+$ and $\boldsymbol{n}^-$, respectively normal to $\partial V_{(i)}^+$ and $\partial V_{(i)}^-$, present the following relation:

$$\boldsymbol{n}^{-} = -\boldsymbol{n}^{+} . \tag{7}$$

Definitively, the periodic boundary condition on $\partial V_{(i)}$ is given as follow:

$$\boldsymbol{u}(\boldsymbol{X}^{+},t) - \boldsymbol{u}(\boldsymbol{X}^{-},t) = (\overline{\boldsymbol{F}}(\overline{\boldsymbol{X}},t) - \boldsymbol{I})(\boldsymbol{X}^{+} - \boldsymbol{X}^{-}) . \tag{8}$$

Imposing the Eq. (8) at the boundary of the RVE, this condition leads to an anti-periodic traction field and to a periodic fluctuation field as expressed in the following:

$$\boldsymbol{t}_R^{+}(\boldsymbol{X},t) = -\boldsymbol{t}_R^{-}(\boldsymbol{X},t) \ , \tag{9}$$

$$\boldsymbol{w}_R^{+}(\boldsymbol{X},t) = \boldsymbol{w}_R^{-}(\boldsymbol{X},t) \ . \tag{10}$$

In order to take into account for frictionless self-contact phenomena between opposite crack surfaces, the following conditions at each point $\boldsymbol{X}_u$ of the upper crack surfaces are introduced:

$$\begin{cases} h^{l}(\boldsymbol{X}^{u} + \boldsymbol{u}(\boldsymbol{X}^{u},t),t) \geq 0 \\ {\sigma_R}^{u}(t) \leq 0 \\ {\sigma_R}^{u}(t)\, h^{l}(\boldsymbol{X}^{u} + \boldsymbol{u}(\boldsymbol{X}^{u},t),t) = 0 \end{cases} \quad \text{on } \Gamma^{u}_{(i)} . \tag{11}$$

As shown in Fig. 2, $h^{u} = 0$ and $h^{l} = 0$ describe the deformed upper and lower crack surfaces, denoted by Γ^{u} and Γ^{l}, while ${\sigma_R}^{u} = \boldsymbol{T}_R \boldsymbol{n}^{u}_{(i)} \bullet \boldsymbol{n}^{u}$ is the normal nominal contact reaction on the upper crack surface, where $\boldsymbol{n}^{u}$ represents the deformed outward normal, and $\boldsymbol{T}_R \boldsymbol{n}^{u}_{(i)} = \boldsymbol{r}^{u}_R$ represents the nominal contact reaction. For sake of brevity, only the equations governing the rate equilibrium solution of the microstructure are reported in the following:

$$\begin{cases} Div\dot{\boldsymbol{T}}_R = \boldsymbol{0} & \text{in } B_{(i)} \\ \dot{\boldsymbol{t}}_R^{+} = -\dot{\boldsymbol{t}}_R^{-} & \text{on } \partial \mathrm{V}_{(i)} \\ \dot{u}_n(\boldsymbol{X})_{\Gamma_C} \leq 0, \ {\sigma_R}^{u} \ \dot{u}_n(\boldsymbol{X})_{\Gamma_C} = 0, \dot{\sigma}^{u}_R \ \dot{u}_n(\boldsymbol{X})_{\Gamma_C} = 0 \text{ and } \dot{\sigma}^{u}_R \leq 0 \ \textit{if} \ \sigma^{u}_R = 0 & \forall \left(\boldsymbol{X}^{l}, \boldsymbol{X}^{u}\right)_C \\ \dot{\boldsymbol{r}}_R^{\,u} \dfrac{dS^{u}_{(i)}}{dS} + \dot{\boldsymbol{r}}_R^{\,l} \dfrac{dS^{l}_{(i)}}{dS} + {\sigma_R}^{u} \boldsymbol{n}^{u} \left(\dfrac{dS^{u}_{(i)}}{dS}\right)^{\cdot} + {\sigma_R}^{l} \boldsymbol{n}^{l} \left(\dfrac{dS^{l}_{(i)}}{dS}\right)^{\cdot} = \boldsymbol{0} & \forall \left(\boldsymbol{X}^{l}, \boldsymbol{X}^{u}\right)_C \\ \dot{\boldsymbol{r}}^{l}_R - \dot{\sigma}^{l}_R \boldsymbol{n}^{l} = \sigma^{l}_R \dot{\boldsymbol{n}}^{l} & \text{on } \Gamma^{l}_{C(i)} \end{cases} \tag{12}$$

where $\dot{u}_n(\boldsymbol{X})$ denotes the projection of the displacement rate along the normal $\boldsymbol{n}^{l}$ to the deformed lower crack surface, $\dot{u}_n(\boldsymbol{X})_{\Gamma_C} = \dot{u}_n(\boldsymbol{X}^{l}) - \dot{u}_n(\boldsymbol{X}^{u})$ represents its jump at a contact point pair $(\boldsymbol{X}^{u}, \boldsymbol{X}^{l})_C$, $\dot{\boldsymbol{r}}_R$ is the nominal contact reaction rate, defined as $\dot{\boldsymbol{r}}_R = \dot{\boldsymbol{T}}_R \boldsymbol{n}_{(i)}$.

To derive the infinitesimal stability and non-bifurcation conditions of the equilibrium configuration, the following contact surface integral is examined:

$$\delta L_{rate}(\Gamma_c) = \int_{\Gamma_{c(i)}{}^{l}} \left[\dot{\boldsymbol{r}}^{l}_R \bullet \delta \boldsymbol{u}^{l}\right] dS_{(i)} + \int_{\Gamma_{c(i)}{}^{u}} \left[\dot{\boldsymbol{r}}^{u}_R \bullet \delta \boldsymbol{u}^{u}\right] dS_{(i)} . \tag{13}$$

representing the virtual work of the contact reaction rate acting on the present contact interface in a virtual displacement $\delta \boldsymbol{u} \in A^{*}(\overline{\boldsymbol{F}}, \overline{\boldsymbol{F}})$.

Using Eq. $(12)_4$ the contact surface integral becomes:

$$\begin{aligned} &\delta L_{rate}(\Gamma_c) = \int_{\Gamma_{c(i)}{}^{l}} \dot{\boldsymbol{r}}_R^{\,l} \bullet \delta \boldsymbol{u}^{l} dS^{l}_{(i)} - \int_{\Gamma_{c(i)}{}^{u}} \left[{\sigma_R}^{l} \boldsymbol{n}^{l} \left(\frac{dS^{l}_{(i)}}{dS}\right)^{\cdot} + \dot{\boldsymbol{r}}_R^{\,l} \frac{dS^{l}_{(i)}}{dS} + {\sigma_R}^{u} \boldsymbol{n}^{u} \left(\frac{dS^{u}_{(i)}}{dS}\right)^{\cdot} \right] \frac{dS}{dS^{u}_{(i)}} \bullet \delta \boldsymbol{u}^{u} dS^{u}_{(i)} = \\ &\int_{\Gamma_{c(i)}{}^{l}} \dot{\boldsymbol{r}}_R^{\,l} \bullet \ \delta \boldsymbol{u}_{\Gamma_c} dS^{l}_{(i)} - \int_{\Gamma_{c(i)}{}^{l}} {\sigma_R}^{l} \left[\left(\frac{dS^{l}_{(i)}}{dS}\right)^{\cdot} \frac{dS}{dS^{l}_{(i)}} - \left(\frac{dS^{u}_{(i)}}{dS}\right)^{\cdot} \frac{dS}{dS^{u}_{(i)}} \right] \delta u_n{}^{l} dS^{l}_{(i)} \end{aligned} \tag{14}$$

and taking into account for the frictionless contact model (see eqn $(12)_5$), the contact reaction rate can be written as $\dot{\boldsymbol{r}}_R = \sigma_R \dot{\boldsymbol{n}} + \dot{\sigma}_R \boldsymbol{n}$ leading to an expression in which the work done by the nominal contact reaction through the virtual displacement consists in two contributions: the first (a) is a contribution related to the tangential component of the nominal contact reaction rate $\sigma_R \dot{\boldsymbol{n}}$ (since $\boldsymbol{n} \bullet \dot{\boldsymbol{n}} = 0$); the second (b) is a contribution related to the different variation of the reference to actual surface element ratio $dS_{(i)}^u / dS$ between the lower and upper crack contact surfaces:

$$\delta L_{rate}(\Gamma_c) = \underbrace{\int_{\Gamma_{c(i)}^l} \sigma_R^l \dot{\boldsymbol{n}}^l \bullet \delta \boldsymbol{u}_{\Gamma_c} \, dS_{(i)}^l}_{a} - \underbrace{\int_{\Gamma_{c(i)}^l} \sigma_R^l \left[\!\!\left[\left(\frac{dS_{(i)}}{dS} \right)^{\cdot} \frac{dS}{dS_{(i)}} \right]\!\!\right]_{\Gamma_c} \delta u_n^l \, dS_{(i)}^l}_{b} . \tag{15}$$

Uniqueness of the rate response is ensured satisfying the following positivity condition:

$$R\left(\dot{\bar{\boldsymbol{F}}}, \dot{\boldsymbol{w}}_1, \dot{\boldsymbol{w}}_2\right) > 0 \qquad \forall \dot{\boldsymbol{w}}^{(1)} \neq \dot{\boldsymbol{w}}^{(2)} \in A^*(\bar{\boldsymbol{F}}, \dot{\bar{\boldsymbol{F}}}) , \tag{16}$$

where $R(\dot{\bar{\boldsymbol{F}}}, \dot{\boldsymbol{w}}_1, \dot{\boldsymbol{w}}_2)$ is the so-called exclusion functional that assumes the following expression:

$$\begin{aligned} R\left(\dot{\bar{\boldsymbol{F}}}, \dot{\boldsymbol{w}}_1, \dot{\boldsymbol{w}}_2\right) = & \int_{B_{(i)}} \boldsymbol{C}^R\left(\boldsymbol{X}, \bar{\boldsymbol{F}}\right) [\nabla \dot{\boldsymbol{w}}^{(1)} - \nabla \dot{\boldsymbol{w}}^{(2)}] \bullet \left(\nabla \dot{\boldsymbol{w}}^{(1)} - \nabla \dot{\boldsymbol{w}}^{(2)}\right) dV_{(i)} - \int_{\Gamma_{C(i)}^l} \sigma_R^l \Delta \dot{\boldsymbol{n}}^l \bullet \Delta \dot{\boldsymbol{w}}_{\Gamma_C} \, dS_{(i)}^l + \\ & + \int_{\Gamma_{C(i)}^l} \sigma_R^l \left[\!\!\left[\Delta\left(\frac{dS_{(i)}}{dS} \right)^{\cdot} \frac{dS}{dS_{(i)}} \right]\!\!\right]_{\Gamma_C} \Delta \dot{w}_n^l \, dS_{(i)}^l \qquad \text{with } \Delta(\cdot) = \cdot^{(1)} - \cdot^{(2)} \end{aligned} \tag{17}$$

where superscripts (1) and (2) refer to two possible rate solutions $\dot{\boldsymbol{u}}^{(i)} = \dot{\bar{\boldsymbol{F}}} \boldsymbol{X} + \dot{\boldsymbol{w}}^{(i)}$ $(i = 1,2)$ associated to the same $\dot{\bar{\boldsymbol{F}}}$.

In addition, the stability condition of the generic equilibrium configuration is obtained by assuming that the rate problem admits only the trivial rate solution $\dot{\boldsymbol{w}} = \boldsymbol{0}$ thus, by coupling the known solution $\dot{\boldsymbol{w}}^{(2)} = \boldsymbol{0}$ with a generic admissible fluctuation field rate $\dot{\boldsymbol{w}}^{(1)} = \dot{\boldsymbol{w}}$, it follows that the stability condition represents a non-bifurcation criterion for the trivial case with $\bar{\boldsymbol{F}}(t) = \boldsymbol{0}$ and the resulting positivity condition is expressed as:

$$S\left(\bar{\boldsymbol{F}}, \dot{\boldsymbol{w}}\right) > 0 \quad \forall \dot{\boldsymbol{w}}(\boldsymbol{x}) \neq \boldsymbol{0} \in A^*(\bar{\boldsymbol{F}}, \dot{\bar{\boldsymbol{F}}} = \boldsymbol{0}) , \tag{18}$$

where $S(\bar{\boldsymbol{F}}, \dot{\boldsymbol{w}})$ is the so-called stability functional assuming the following expression:

$$S\left(\bar{\boldsymbol{F}}, \dot{\boldsymbol{w}}\right) = \int_{B_{(i)}} \boldsymbol{C}^R\left(\boldsymbol{X}, \bar{\boldsymbol{F}}\right) [\nabla \dot{\boldsymbol{w}}] \bullet \nabla \dot{\boldsymbol{w}} dV_{(i)} - \int_{\Gamma_{C(i)}^l} \sigma_R^l \dot{\boldsymbol{n}}^l \bullet \dot{\boldsymbol{w}}_{\Gamma_C} \, dS_{(i)}^l + \int_{\Gamma_{C(i)}^l} \sigma_R^l \left[\!\!\left[\left(\frac{dS_{(i)}}{dS} \right)^{\cdot} \frac{dS}{dS_{(i)}} \right]\!\!\right]_{\Gamma_C} \dot{w}_n^l \, dS_{(i)}^l . \tag{19}$$

Further details about the stability and non-bifurcation conditions can be found in (Greco, 2013; Greco et al., 2016). In the general case of non-homogeneous loading $\bar{\boldsymbol{F}}_{(0)} \neq \boldsymbol{0}$ owing to contact nonlinearities, the stability condition does not ensure uniqueness since an eigenstate does not correspond to a primary bifurcation state; on the other hand the non-bifurcation condition (17) implies stability. In order to circumvent non-linearities arising from crack self-contact, incrementally linear comparison problems can be adopted as shown in (Greco, 2013), specifically, a lower bound predictions for the loading levels at the onset of instability and bifurcation can be obtained by using the incremental comparison problem corresponding to the completely free to penetrate rate conditions over the whole crack contact interface, in other words $\left[\!\!\left[\dot{w}_{(0)n} \right]\!\!\right]_{\Gamma_C}$ is assumed arbitrary on the whole Γ_c.

3. Microscopic stability analysis by means of multiscale techniques

The previously developed theoretical formulation is here applied to analyze the macroscopic compressive failure behavior of defected periodic fiber-reinforced composites subjected to large deformations associated to the coupled effects of microscopic instabilities and microfractures. In particular, a semiconcurrent multiscale model (FE^2-like) was adopted, in which the macroscopic constitutive response of the composite structure was extracted (for each Newton-

Raphson iteration) by solving a microscopic boundary value problem linked at the macroelements of the homogenized domain. The information are transferred on the fly during the simulation from lower (micro) to higher (macro) scales and vice versa establishing a "two-way" weak coupling, similarly to the FE^2 method (see Fig. 3).

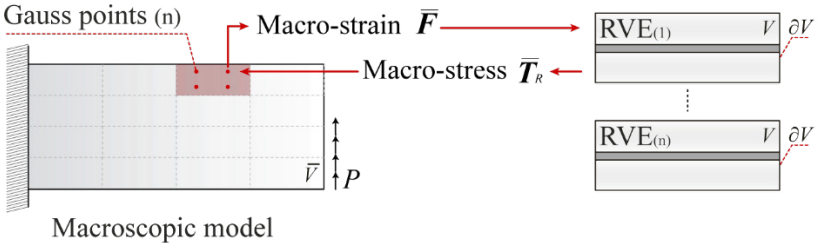

Fig. 3. Schematic representation of the (FE^2) semiconcurrent multiscale approach.

It is worth noting that the microscopic problems are decoupled to each other leading to a lower computational effort only in presence of an effective core processor parallelization adequately implemented in the solver procedure. However, in order to avoid the evaluation of the critical load at each load step through an eigenvalue problem, it is possible to use the two-dimensional stability and uniqueness domains reported in the following works: (Greco et al., 2018b, 2018a). The drawback of this approach is the difficulty to evaluate the boundary layer effects, if a first order homogenization scheme is used. Below, in order to demonstrate both accuracy and validity of the previously described theoretical formulation within a multiscale analysis framework, some numerical applications were reported.

3.1 Multiscale analysis of defected fiber-reinforced composites subjected to homogeneous macroscopic deformations

The first multiscale application considers a composite material reinforced with continuous fibers arranged according to a unidirectional pattern. The homogenized domain, length 300 μm and high 100 μm, is subjected to a homogeneous compressive uniaxial macro-deformation path in the fiber direction (Fig. 4). In the semiconcurret multiscale framework, the microscopic periodic unit cells are connected to the homogenized continuum in order to obtain the macroscopic response along the primary macro-deformation path. In the meantime, the macro-deformation state of each microscopic cell has been monitored by means of the two-dimensional stability and uniqueness domains presented in (Greco et al., 2018b, 2018a). The obtained critical load factor t_c^H is equal to 0.1139.

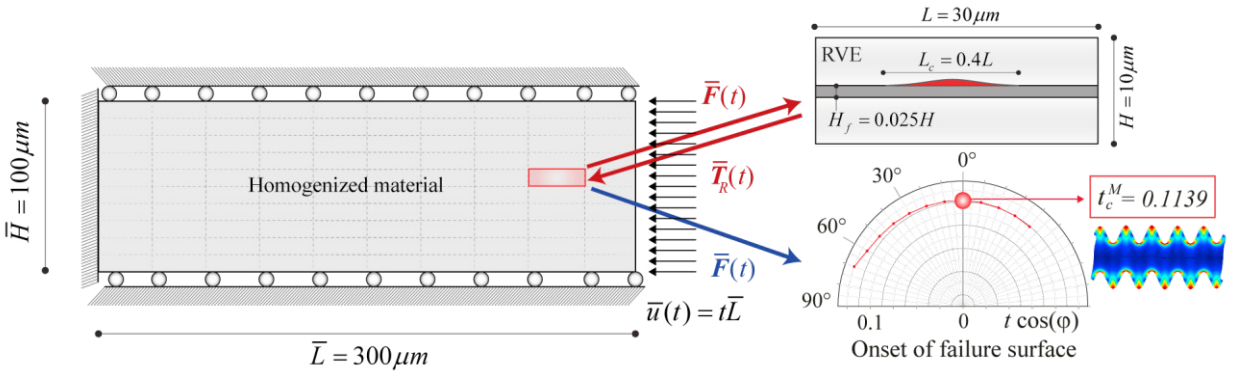

Fig. 4. A composite material reinforced with continuous fibers subjected to homogeneous compressive uniaxial macro-deformation path and check of critical deformation through 2D stability and uniqueness domains.

A convergence analysis, reported in Fig. 5, to the RVE size has been incorporated in the numerical procedure to assess the local nature of the instability mode and, as a consequence, to verify the correspondence between the repeated unit cell (RUC) and the representative volume element (RVE). In detail, the coincidence of the mode shape and the critical load level between a single cell and a cell assembly of increasing dimensions (2x2 and 4x4), were verified.

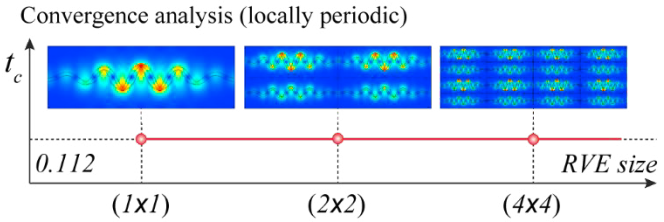

Fig. 5. Convergence analysis to the RVE size incorporated in the numerical procedure.

To evaluate the accuracy and the effectiveness of the adopted multiscale model, the obtained results have been compared with the stability analysis performed on a direct numerical model based on the explicit discretization of the heterogeneities of the composite microstructure. The direct numerical analysis has been developed by solving in a coupled way the global and the rate eigenvalue boundary value problems (Fig. 6) providing the bifurcation and the instability load levels for the exact formulation. The obtained critical load parameter value is equal to 0.1172.

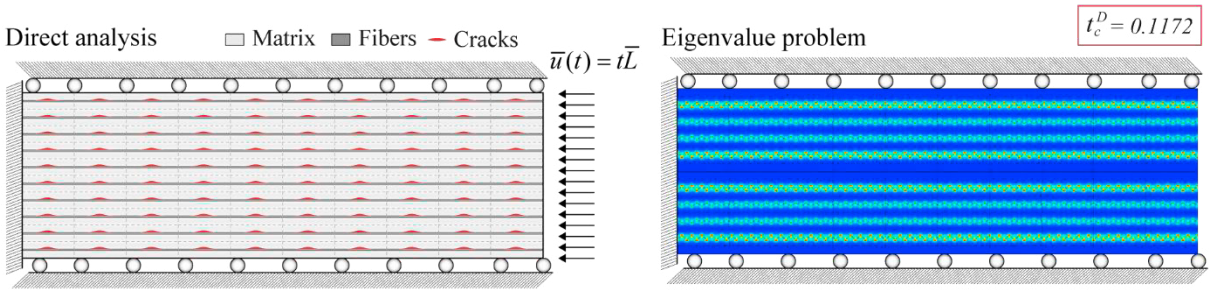

Fig. 6. Direct numerical analysis of a fiber-reinforced composite material subjected to homogeneous macro deformation with the accompanying nonlinear eigenmode boundary value problems giving the bifurcation and the instability critical load factor.

The results are reasonably accurate when compared with the critical load predictions of the direct numerical analysis. The relative percentage error of the critical load level, about of 3%, is due to the boundary layers effects induced by the external constrains.

3.2 Multiscale analysis of fiber-reinforced composites subjected to nonhomogeneous macroscopic deformations

The second application concerns a cantilever composite beam reinforced with continuous fibers, length 240 μm and high 40 μm, subjected to a bending stress induced by a concentrated vertical force applied at the free end of the beam leading to a macroscopic displacement $\bar{u}(t)$. The numerical analysis of the homogenized model, composed by a 4x8 periodic unit cell assembly (see Fig. 7), was conducted assuming quasi-static displacement-controlled loading conditions. The dimensions of the considered unit cell, denotes as L and H, are chosen such that their ratio L/H is equal to 3 and L is equal to 30 μm, whereas the thickness of the fiber (i.e. the reinforcement layer), denoted as H_f, is set as $0.025H$, associated with a fiber volume fraction of 2.5%. The length of preexisting crack is equal to $0.4L$.

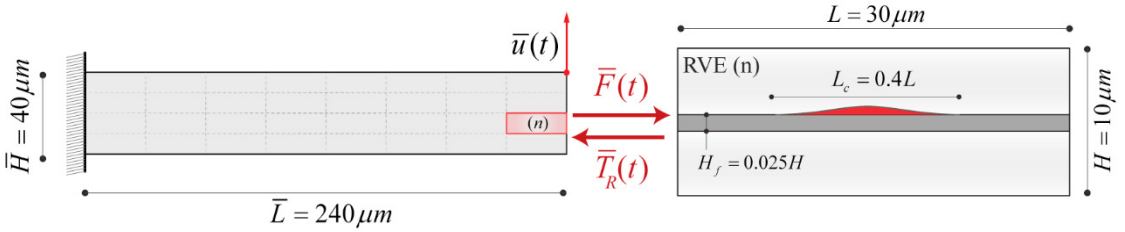

Fig. 7. A cantilever composite beam reinforced with continuous fibers and subjected to concentrated vertical force at the free end of the beam leading to a macroscopic displacement.

In the Fig. 8a, the Von Mises stress map of the macroscopic multiscale model is reported together with their linked microscopic representative volume elements (32 RVEs). In addition, the zoom on the critical cell, together with the vertical reaction versus the macro displacement $\bar{u}(t)$ plot, are reported at the left bottom side.

It worth noting that such curve shows a load jump in correspondence with the critical load factor, that is about of 30.1μ. It was measured by means of a graphic extrapolation reported in the top side of Fig. 8b. However, in order to evaluate the accuracy of the multiscale model predictions, the lower bound of the primary instability and bifurcation load was assessed through a linear comparison problem allowing for incremental crack surface penetration (bottom side of Fig. 8b).

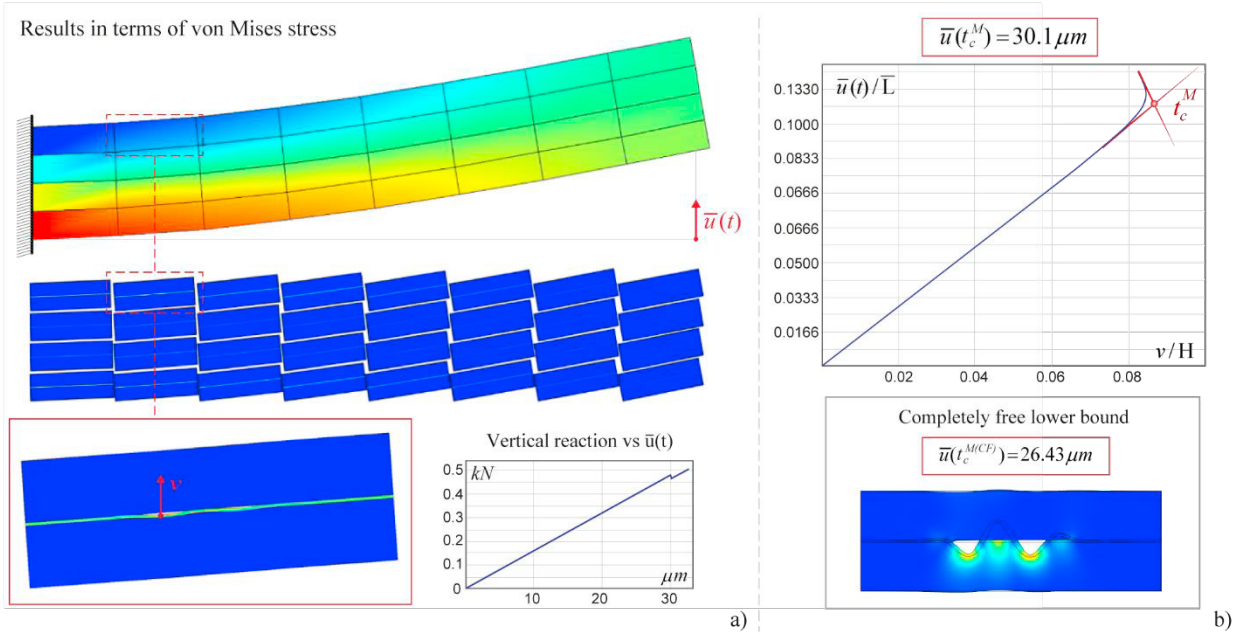

Fig. 8. Multiscale numerical simulation on a cantilever beam subjected to nonhomogeneous deformation (a). Graphical extrapolation of the instability critical load factor and assessment to the limit bound obtained through eigenvalue problem (b).

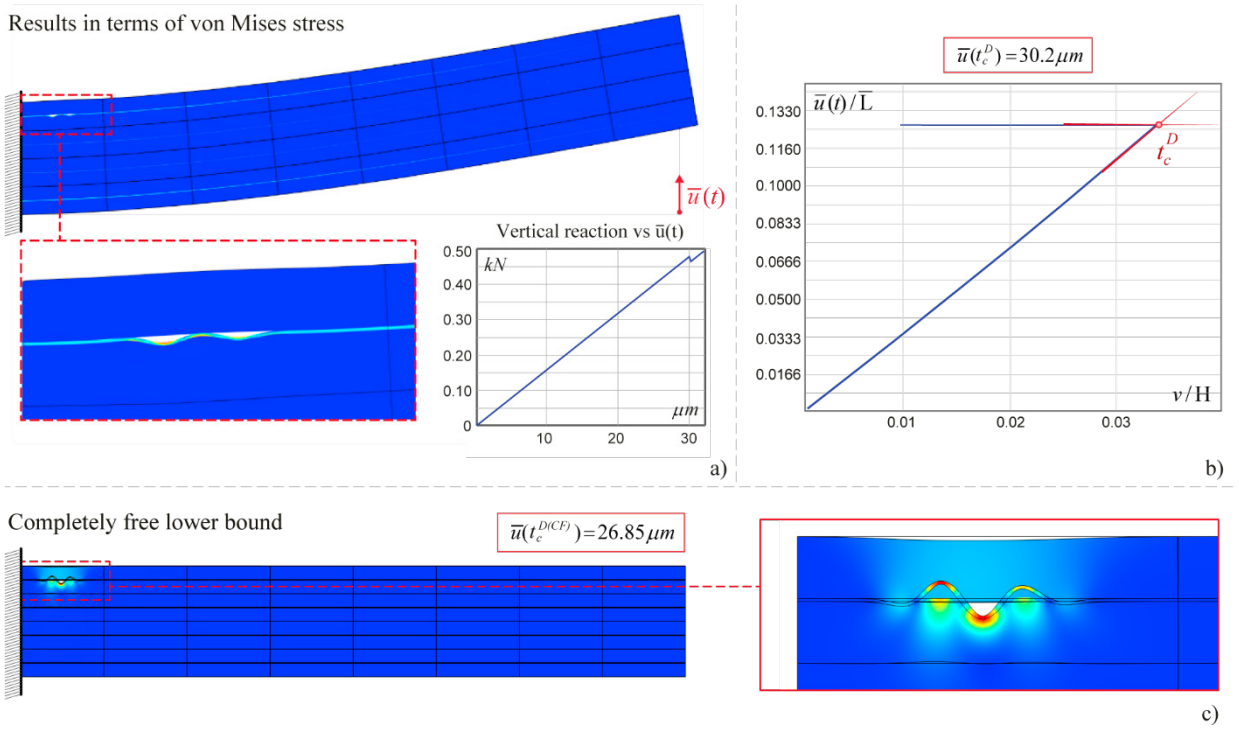

Fig. 9. Direct numerical simulation on a cantilever beam subjected to nonhomogeneous deformation (a). Graphical extrapolation of the instability critical load factor (b) and assessment to the lower bound obtained through eigenvalue problem (c).

The evaluated lower bound value is equal to 26.43μm. A comparison between results of multiscale and direct numerical simulation, are discussed here. The Fig. 9a shows the Von Mises stress map at the onset of microscopic instability of the direct model together with the vertical reaction versus the macro displacement $\overline{u}(t)$ plot. The critical load factor, obtained by a graphic extrapolation (Fig. 9b) and the evaluated lower bound by means of eigenvalue problem (Fig. 9c) are equal to 30.2 μm and 26.85 μm, respectively. As in the multiscale analysis, a load jump in the loading curve of direct numerical simulation occurs (bottom side of Fig. 9a). As expected in both multiscale and direct analysis the obtained lower bound of the primary instability and bifurcation load is lower than the exact critical load factor. The relative percentage errors between the two different simulations in term of both lower bound and exact critical load are 1.54% and 0.33%, respectively. Such numerical results demonstrated the capability and the effectiveness of adopted multiscale model to predict the critical loads for primary instability and bifurcation in defected fiber-reinforced composite materials subjected to both homogeneous and nonhomogeneous macroscopic deformations.

4. Conclusions

In this work the microscopic failure mechanisms triggered by fiber microbuckling were investigated for fiber-reinforced periodic composites containing microscopic defects; these phenomena are of central importance for an accurate prediction of the load carrying capacity in the presence of compression along the fiber direction in unidirectional fiber-reinforced or layered composites. As a matter of fact, the interaction between micro-fractures and buckling instabilities may lead to a strong decrease in the compressive strength of the composite material with a premature failure of the composite solid.

With the aim to perform an accurate analysis of the above-mentioned failure behavior a rigorous full finite deformation continuum formulation was proposed to account for the interaction between local fiber buckling and matrix or fiber/matrix interface microcracks by modeling unilateral self-contact along crack surfaces in a multiscale

framework. The adopted formulation made it possible to highlight the presence of non-standard rate contributions arising from crack self-contact interface mechanisms that play a fundamental role in the prediction of the microscopic critical load of the composite solid. To this end, the first part of the paper is devoted to the theoretical formulation of instability and bifurcation phenomena for microcracked composite materials subjected to a macrostrain driven loading path. Then, with the aim to demonstrate that the developed formulation can be adopted in the context of multiscale approaches for predicting the failure behavior of locally periodic defected composite solids subjected to large deformations, some practical application was performed adopting a semiconcurrent two-scale approach, in which the macroscopic constitutive law is evaluated resolving a BVP in each macroelement of the homogenized domain.

Numerical applications carried out for macroscopic loadings involving both homogeneous and inhomogeneous deformations in the homogenized solid, show that a two-scale homogenization approach is able to give accurate predictions of the critical load level associated to microscopic instabilities or bifurcations, as confirmed via comparisons with a direct analysis with an explicit meshing of all heterogeneities.

Acknowledgements

Fabrizio Greco gratefully acknowledges financial support from the Italian Ministry of Education, University and Research (MIUR) under the P.R.I.N. 2017 National Grant “Multiscale Innovative Materials and Structures” (Project Code 2017J4EAYB; University of Calabria Research Unit).

References

Bruno, D., Greco, F., Lonetti, P., Nevone Blasi, P., 2008. Influence of micro-cracking and contact on the effective properties of composite materials. Simulation Modelling Practice and Theory 16, 861–884. https://doi.org/10.1016/j.simpat.2008.05.006

De Maio, U., Fabbrocino, F., Greco, F., Leonetti, L., Lonetti, P., 2019a. A study of concrete cover separation failure in FRP-plated RC beams via an inter-element fracture approach. Composite Structures 212, 625–636. https://doi.org/10.1016/j.compstruct.2019.01.025

De Maio, U., Greco, F., Leonetti, L., Luciano, R., Nevone Blasi, P., Vantadori, S., 2019b. A refined diffuse cohesive approach for the failure analysis in quasibrittle materials—part I: Theoretical formulation and numerical calibration. Fatigue Fract Eng Mater Struct ffe.13107. https://doi.org/10.1111/ffe.13107

De Maio, U., Greco, F., Leonetti, L., Luciano, R., Nevone Blasi, P., Vantadori, S., 2019c. A refined diffuse cohesive approach for the failure analysis in quasibrittle materials—part II: Application to plain and reinforced concrete structures. Fatigue Fract Eng Mater Struct 42, 2764–2781. https://doi.org/10.1111/ffe.13115

Fantuzzi, N., Leonetti, L., Trovalusci, P., Tornabene, F., 2018. Some Novel Numerical Applications of Cosserat Continua. Int. J. Comput. Methods 15, 1850054. https://doi.org/10.1142/S0219876218500548

Feo, L., Greco, F., Leonetti, L., Luciano, R., 2015. Mixed-mode fracture in lightweight aggregate concrete by using a moving mesh approach within a multiscale framework. Composite Structures 123, 88–97. https://doi.org/10.1016/j.compstruct.2014.12.037

Feyel, F., Chaboche, J.-L., 2000. FE2 multiscale approach for modelling the elastoviscoplastic behaviour of long fibre SiC/Ti composite materials. Computer Methods in Applied Mechanics and Engineering 183, 309–330. https://doi.org/10.1016/S0045-7825(99)00224-8

Geymonat, G., Muller, S., Triantafyllidis, N., 1993. Homogenization of nonlinearly elastic materials, microscopic bifurcation and macroscopic loss of rank-one convexity. Archive for Rational Mechanics and Analysis 122, 231–290. https://doi.org/10.1007/BF00380256

Greco, F., 2013. A study of stability and bifurcation in micro-cracked periodic elastic composites including self-contact. International Journal of Solids and Structures 50, 1646–1663. https://doi.org/10.1016/j.ijsolstr.2013.01.036

Greco, F., 2009. Homogenized mechanical behavior of composite micro-structures including micro-cracking and contact evolution. Engineering Fracture Mechanics 76, 182–208. https://doi.org/10.1016/j.engfracmech.2008.09.006

Greco, F., Leonetti, L., Lonetti, P., Nevone Blasi, P., 2015. Crack propagation analysis in composite materials by using moving mesh and multiscale techniques. Computers & Structures 153, 201–216. https://doi.org/10.1016/j.compstruc.2015.03.002

Greco, F., Leonetti, L., Luciano, R., Nevone Blasi, P., 2016. Effects of microfracture and contact induced instabilities on the macroscopic response of finitely deformed elastic composites. Composites Part B: Engineering 107, 233–253. https://doi.org/10.1016/j.compositesb.2016.09.042

Greco, F., Leonetti, L., Medaglia, C.M., Penna, R., Pranno, A., 2018a. Nonlinear compressive failure analysis of biaxially loaded fiber reinforced materials. Composites Part B: Engineering 147, 240–251. https://doi.org/10.1016/j.compositesb.2018.04.006

Greco, F., Leonetti, L., Nevone Blasi, P., 2014. Adaptive multiscale modeling of fiber-reinforced composite materials subjected to transverse microcracking. Composite Structures 113, 249–263. https://doi.org/10.1016/j.compstruct.2014.03.025

Greco, F., Leonetti, L., Pranno, A., Rudykh, S., 2020. Mechanical behavior of bio-inspired nacre-like composites: A hybrid multiscale modeling approach. Composite Structures 233, 111625. https://doi.org/10.1016/j.compstruct.2019.111625

Greco, F., Lonetti, P., Luciano, R., Nevone Blasi, P., Pranno, A., 2018b. Nonlinear effects in fracture induced failure of compressively loaded fiber reinforced composites. Composite Structures 189, 688–699. https://doi.org/10.1016/j.compstruct.2018.01.014

Greco, F., Luciano, R., 2011. A theoretical and numerical stability analysis for composite micro-structures by using homogenization theory. Composites Part B: Engineering 42, 382–401. https://doi.org/10.1016/j.compositesb.2010.12.006

Li, J., Slesarenko, V., Rudykh, S., 2019. Microscopic instabilities and elastic wave propagation in finitely deformed laminates with compressible hyperelastic phases. European Journal of Mechanics - A/Solids 73, 126–136. https://doi.org/10.1016/j.euromechsol.2018.07.004

Li, S., Wang, G., Morgan, E., 2004. Effective elastic moduli of two dimensional solids with distributed cohesive microcracks. European Journal of Mechanics - A/Solids 23, 925–933. https://doi.org/10.1016/j.euromechsol.2004.07.002

Michel, J.C., Lopez-Pamies, O., Ponte Castañeda, P., Triantafyllidis, N., 2010. Microscopic and macroscopic instabilities in finitely strained fiber-reinforced elastomers. Journal of the Mechanics and Physics of Solids 58, 1776–1803. https://doi.org/10.1016/j.jmps.2010.08.006

Miehe, C., Schröder, J., Becker, M., 2002. Computational homogenization analysis in finite elasticity: material and structural instabilities on the micro- and macro-scales of periodic composites and their interaction. Computer Methods in Applied Mechanics and Engineering 191, 4971–5005. https://doi.org/10.1016/S0045-7825(02)00391-2

Nestorović, M.D., Triantafyllidis, N., 2004. Onset of failure in finitely strained layered composites subjected to combined normal and shear loading. Journal of the Mechanics and Physics of Solids 52, 941–974. https://doi.org/10.1016/j.jmps.2003.06.001

Nezamabadi, S., Yvonnet, J., Zahrouni, H., Potier-Ferry, M., 2009. A multilevel computational strategy for handling microscopic and macroscopic instabilities. Computer Methods in Applied Mechanics and Engineering 198, 2099–2110. https://doi.org/10.1016/j.cma.2009.02.026

Slesarenko, V., Rudykh, S., 2017. Microscopic and macroscopic instabilities in hyperelastic fiber composites. Journal of the Mechanics and Physics of Solids 99, 471–482. https://doi.org/10.1016/j.jmps.2016.11.002

Triantafyllidis, N., Maker, B.N., 1985. On the Comparison Between Microscopic and Macroscopic Instability Mechanisms in a Class of Fiber-Reinforced Composites. Journal of Applied Mechanics 52, 794. https://doi.org/10.1115/1.3169148

Tuna, M., Leonetti, L., Trovalusci, P., Kirca, M., 2019. 'Explicit' and 'implicit' non-local continuous descriptions for a plate with circular inclusion in tension. Meccanica. https://doi.org/10.1007/s11012-019-01091-3

Yu, K., Hu, H., Chen, S., Belouettar, S., Potier-Ferry, M., 2013. Multi-scale techniques to analyze instabilities in sandwich structures. Composite Structures 96, 751–762. https://doi.org/10.1016/j.compstruct.2012.10.007